The Re-emergence of SST Anomalies in the North Pacific Ocean

MICHAEL A. ALEXANDER*

Climate Diagnostics Center, CIRES, University of Colorado, Boulder, CO

CLARA DESER

National Center for Atmospheric Research, Boulder CO

MICHAEL S. TIMLIN

Climate Diagnostics Center, CIRES, University of Colorado, Boulder, CO

* Corresponding author's address:
CDC-CIRES, Box 449
University of Colorado
Boulder, Colorado 80309
maa@cdc.noaa.gov

Submitted to the Journal of Climate
October, 1997

ABSTRACT

Sea surface temperature (SST) data and two different upper ocean temperature analyses are used to study the winter-to-winter recurrence of SST anomalies in the North Pacific Ocean. The SSTs recur when temperature anomalies that form in the deep ocean mixed layer in late winter/early spring are isolated from the atmosphere in the summer seasonal thermocline and then re-emerge at the surface when the mixed layer deepens during the following fall/winter. This "re-emergence mechanism" is evaluated over the basin by correlating the time series of the leading pattern of ocean temperature anomalies in the summer seasonal thermocline (~60-85 m in August-September) with SST anomalies over the course of the year. The results indicate that the dominant large-scale SST anomaly pattern that forms in the North Pacific during late winter, with anomalies of one sign in the central Pacific and the opposite sign along the coast of North America, is sequestered in the seasonal thermocline in summer and returns to the surface in the following fall, with little persistence at the surface in the summer.

Regions in the east, central, and west Pacific all show signs of the re-emergence process, but indicate that it is influenced by the timing and amplitude of the mean seasonal cycle in mixed layer depth. The maximum mixed layer depth increases from east to west across the basin: as a result, the thermal anomalies are shallower and return to the surface sooner in the east compared with the west Pacific. At some locations, the re-emerging signal is also influenced by when the SST anomalies are created. In the east Pacific, SST anomalies that are initiated in February-March extend through a deeper mixed layer, persist at greater depths in summer, and are then re-entrained later in the year compared with those initiated in April-May.

This page left intentionally blank.

1. Introduction

Recently, a host of observational and modeling studies have documented interannual through decadal variability in midlatitude atmosphere-ocean system (Tanimoto 1993; Trenberth and Horrel 1994; Yukimoto et al. 1996; Zhang et al. 1997; Mantua et al. 1997; etc.). The physical mechanisms used to explain decadal variability generally involve ocean dynamics. Many studies have found decadal oscillations associated with the thermohaline circulation in the North Atlantic (e.g. Weaver et al. 1991; Delworth et al. 1993; Capatondi and Holland 1997). Several mechanisms have also been proposed to explain decadal variability in the North Pacific including oscillations in the ocean heat transport in the subtropical gyre which is sustained by positive atmosphere-ocean feedback (Latif and Barnett 1994, 1996; Robertson 1996; Jin 1997; Zhang and Levitus 1997); slowly propagating oceanic Rossby waves excited by stochastic surface wind stress forcing (Frankignoul et al. 1997; Zorita and Frankignoul 1997); poleward propagating Kelvin waves associated with El Niño events (Jacobs et al. 1994; Meyers et al. 1996); and tropical-extratropical interactions through both the atmosphere and the ocean (Gu and Philander 1997).

In contrast, interannual variability in sea surface temperature (SST) has mainly been attributed to local thermodynamic interactions between the atmosphere and upper ocean (Gill and Niiler 1972; Frankignoul and Reynolds 1983; Frankignoul 1985; Battisti et al. 1995, Delworth 1996). Once created, ocean temperature anomalies in the surface mixed layer (~20-500 m) can be sustained for several months due to the large heat capacity of sea water. Frankignoul and Hasselman (1976), Alexander and Penland (1996), and Hall and Manabe (1996) showed that away from regions with strong currents much of the variability in midlatitude SSTs on monthly and longer timescales can result from the ocean mixed layer being forced by surface heat fluxes associated with storms. The SST anomalies which develop are damped by a negative linear feedback which represents the enhanced (reduced) loss of heat from anomalous warm (cold) waters. However, much of the heat associated with anomalous sea-to-air fluxes remains in the atmospheric boundary layer, as a result the surface air temperature adjusts to the underlying ocean, reducing the negative feedback. This process, termed "reduced thermal damping" by Barsugli and Battisti (1997), enables SST and near-surface air temperature anomalies to persist longer, the latter has been demonstrated by comparing atmospheric general circulation model (AGCM) simulations in which the atmosphere is coupled to an ocean model to those in which the climatological SSTs are specified as boundary conditions (Blade 1997; Bhatt et al., 1997; Saravanan and McWilliams 1997).

Thermodynamic feedbacks between marine stratus clouds and SSTs may also enhance the persistence of midlatitude SST anomalies, especially in summer. Klein and Hartmann (1993), Norris and Leovy (1994), Weare et al. (1994) and Klein et al. (1995) have shown that there is a strong positive feedback between anomalies in the large-scale SST pattern and low-level stratus clouds: an increase in stratus clouds reduces the solar radiation reaching the surface, which reduces SST and thereby increases the static stability of the boundary layer – a factor that tends to enhance cloudiness. Zhang et al. (1997) and Norris et al. (1997) have suggested that this positive feedback can lead to persistence of SST anomalies from both summer to winter and winter to summer.

Local processes within the upper ocean, such as the seasonal variation in the depth of the surface mixed layer, may also lead to SST variability. In response to the seasonal cycle in wind stirring and surface buoyancy forcing the ocean mixed layer deepens through fall and winter and then reforms close to the surface in spring and remains shallow through late summer. Elsberry and Garwood (1978) and Lanzante and Harnack (1983) found some indications that when the mixed layer shoaled in spring could influence summertime SSTs. If, for example, the mixed layer shoaled earlier than normal it would become anomalously warm by summer as the net surface heating was distributed over a thinner layer.

Namias and Born (1970, 1974) were the first to note a tendency for midlatitude SST anomalies to recur from one winter to the next without persisting through the intervening summer. They speculated that temperature anomalies that form at the surface and spread throughout the deep winter mixed layer remain beneath the mixed layer when it shoals in spring. The thermal anomalies are then incorporated into the stable summer seasonal thermocline where they are insulated from surface fluxes. When the mixed layer deepens again in the following fall, the anomalies are re-entrained into the surface layer and influence the SST. This "re-emergence mechanism" was examined in greater detail by Alexander and Deser (1995) using subsurface temperature data and one dimensional mixed layer model simulations at a few weather stations in the North Atlantic and North Pacific Oceans. They found that the winter-to-winter re-emergence of SST anomalies occurred at several locations remote from strong ocean currents. Evidence for the re-emergence mechanism was also found by Miller et al. (1994) using a primitive equation ocean model forced by observed surface flux anomalies, Alexander and Penland where a one-dimensional ocean model was driven by stochastic atmo-

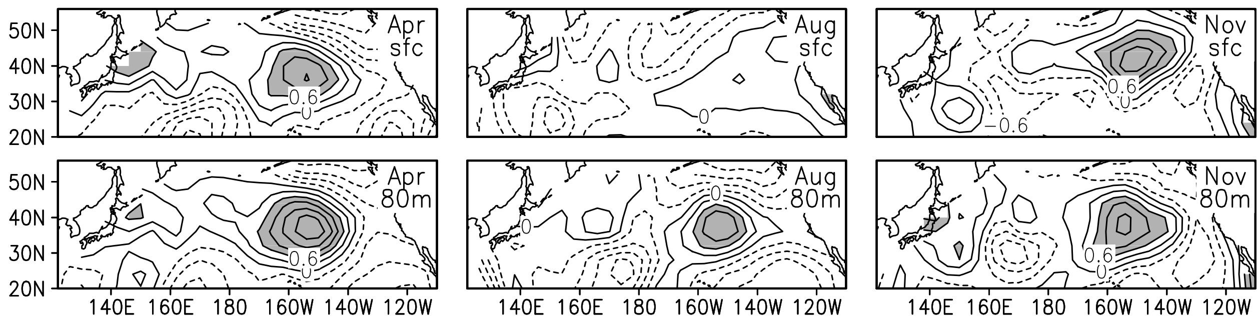

Fig. 1. Monthly temperature anomalies (˚C) in the North Pacific in 1972 during the months of April, August, and November at the surface (top row) and 80 m (bottom row). The temperature values are from the analyses of White (1995) with values grater than 0.6 shaded.

spheric forcing, and Bhatt et al. (1997) in a simulation where a mixed layer ocean model was coupled to an AGCM.

In the present study, we expand on the work of Alexander and Deser (1995) by examining the extent to which the re-emergence mechanism occurs over the North Pacific Ocean using observed temperature fields. A possible occurrence of the re-emergence mechanism over the North Pacific is presented in Fig. 1, which shows the monthly temperature anomalies in April, August, and November at the surface and at 85 m depth during 1972. The temperature anomaly pattern at the surface in August is markedly different from all of the others which each have warm water near 40°N, 150°W surrounded by cold water. While Fig. 1 suggests a link between SST anomalies in the spring and fall via the summer thermocline, several key questions about the re-emergence process remain. Is the re-emergence mechanism wide spread or is its just found at a few locations? Are the anomalies that partake in the re-emergence mechanism related to the dominant patterns of SST variability either in the winter when they are initiated or when they return to the surface in the following fall/winter? Does the timing and strength of the re-emerging signal depend on when or where the SST anomaly was initially created? We will seek to address these questions by applying several statistical methods to a combination of ocean datasets. The datasets used here are described in section 2, the results are presented in section 3, and then summarized and discussed in section 4.

2. Data Sets

In order to resolve the re-emerging signal across the North Pacific we require basin-wide temperature fields on a monthly basis. However, this resolution is not possible with existing archives of raw data, given that there is an order of magnitude fewer upper ocean temperature profiles than SST observations. One way to enhance the data coverage and obtain the necessary spatial and temporal

Table 1. Characteristics of the three ocean datasets used in this study.

Datasets	Interpolation method	Period of record used	Level depths (m) in the upper 200m	Original Domain	Original Resolution	Final Resolution	Comments
NCEP	GCM-based Assimilation System	1/1980 - 6/1995	5 15 25 35 45 55 65 75 85 95 106 120 136 155 177	35°S-45°N in the Pacific	1°lat x 1.5°lon	4°lat x 4°lon	•enhanced by model & other data •short record •domain ends at 45°N
White	Optimum Interpolation	1969 - 1994	0 20 40 60 80 100 120 160 200	60°S-60°N all oceans	2°lat x 5°lon	4°lat x 4°lon	•fairly long record •spans North Pacific •smoothed in space and time
Smith	EOF Projections	1950 - 1996	surface	global	2°lat x 2°lon (1950-92) 1°lat x 1°lon (1993-96)	4°lat x 4°lon	•long recond •spans North Pacific •surface only

resolution is to combine the ocean data with a dynamical ocean model forced by observed atmospheric conditions, while a second is to apply a statistical interpolation method to fill data voids. In this study, we use ocean temperature analyses produced by each method, the ocean data assimilation system at the National Center for Environmental Prediction (NCEP) and the optimum interpolation scheme devised by Warren White at Scripps Institute of Oceanography. We use both of these data sets as they have different strengths: the data from NCEP analyses use models and other datasets to augment the subsurface temperature information, while White's analyses incorporates only subsurface temperature data but covers more of the North Pacific for a longer period of record. We will also use the SST data from Smith et al. (1996) in conjunction with the subsurface datasets to document the re-emergence mechanism in the North Pacific. The characteristics of the three analyses, referred to here as the NCEP, White, and Smith datasets, are shown in Table 1.

The NCEP assimilation system consists of a modified version of the ocean general circulation model (GCM) developed at the Geophysical Fluid Dynamics Laboratory (GFDL) which incorporates observations of SST taken from satellites and ships, plus subsurface thermal profiles obtained from expendable bathythermographs (BTs). Model fields are stored on a 1.0° latitude by 1.5° longitude grid in the Pacific between 35°S and 45°N, and the upper ocean is well resolved with 10 (15) levels in the upper 100 (200) m. We assume that the temperature obtained from the top level, located 5 m below the surface, is representative of the SST. We use monthly mean temperatures from the assimilation system from its start in January of 1980 through June of 1995. A more complete description of the data assimilation system is given in Derber and Rosati (1989) and Ji et al. (1995).

White (1995) uses optimum interpolation, a statistical method, to obtain gridded temperature analyses from a weighted average of the in situ measurements. Given that nearby observations do not provide independent information, the weighting functions seek to minimize the least-square estimate of the correlation error, where the correlation structure is fit using an auto-regressive model that decreases exponentially in both space and time from a given gridpoint. The observations include mechanical and expendable BTs and station data that have been vertically interpolated to 5 (8) standard levels between the surface and 100 (200) m. The optimal interpolation produces a field of temperature anomalies on a 2° latitude by 5° longitude grid from 60°S-60°N for the years 1955-1994. We have used these analyses starting in 1969, when the amount of data appeared to be sufficient to adequately define temperature anomaly patterns in the North Pacific Ocean.

The SST dataset from Smith et al. (1996) is based on a set of spatial patterns defined by empirical orthogonal functions (EOFs) which are fit to previously grided temperature data. This interpolation method fills data voids and create fields which emphasize large-scale features. The EOFs are based on the period 1982-1993 when satellite measurements of SST are available and then applied to a longer data record. Global monthly SST fields are available from the Smith analyses on a 2°x2° grid for 1950-1992 and on a 1°x1° for 1993-1996.

Each dataset was placed on a 4°x4° grid by weighting the original grid square values by the fraction which fell within a given 4°x4° box. We focus, on the Pacific from 20°N to the northern edge of the domain which is 44°N in the NCEP analyses and the coastal boundaries in the other two data sets. All of our analyses have been calculating using monthly anomalies, defined as the departure of the mean value for a given month from the long term mean of that data set for the NCEP and Smith data sets. The monthly anomalies in the White data are relative to the long term annual mean and a Fourier fit to the annual cycle for the period 1980-89; the anomalies are then adjusted to have a zero mean.

Several different statistical analyses including lead-lag correlations and regressions, EOFs, and extended EOFs (EEOFs) are used to examine the re-emergence mechanism in the North Pacific Ocean. The results from the EOF and EEOF analyses are presented as the correlation between the principal component (PC), the time series associated with the EOF, with the values at the individual grid points. We also use correlation analyses to characterize the temperature variations as a function of depth and season in selected regions of the North Pacific. The statistical significance of the magnitude of correlation coefficients is assessed using a two-tailed t-test and taking into account the autocorrelation in the data according to Quenouille (1954). The 95% significance level is roughly 0.6, 0.5, and 0.4 for the NCEP, White, and Smith data, respectively. However, these levels are approximate given that i) the autocorrelation varies with location, ii) in some cases we are calculating the correlation of the time series of a pattern with that of an individual grid point, and iii) the actual data has been interpolated to gridpoints.

3. Results

a. basin-wide analyses

As a first step in evaluating the re-emergence mechanism over the North Pacific we analyze the evolution of SST anomalies using extended empirical orthogonal

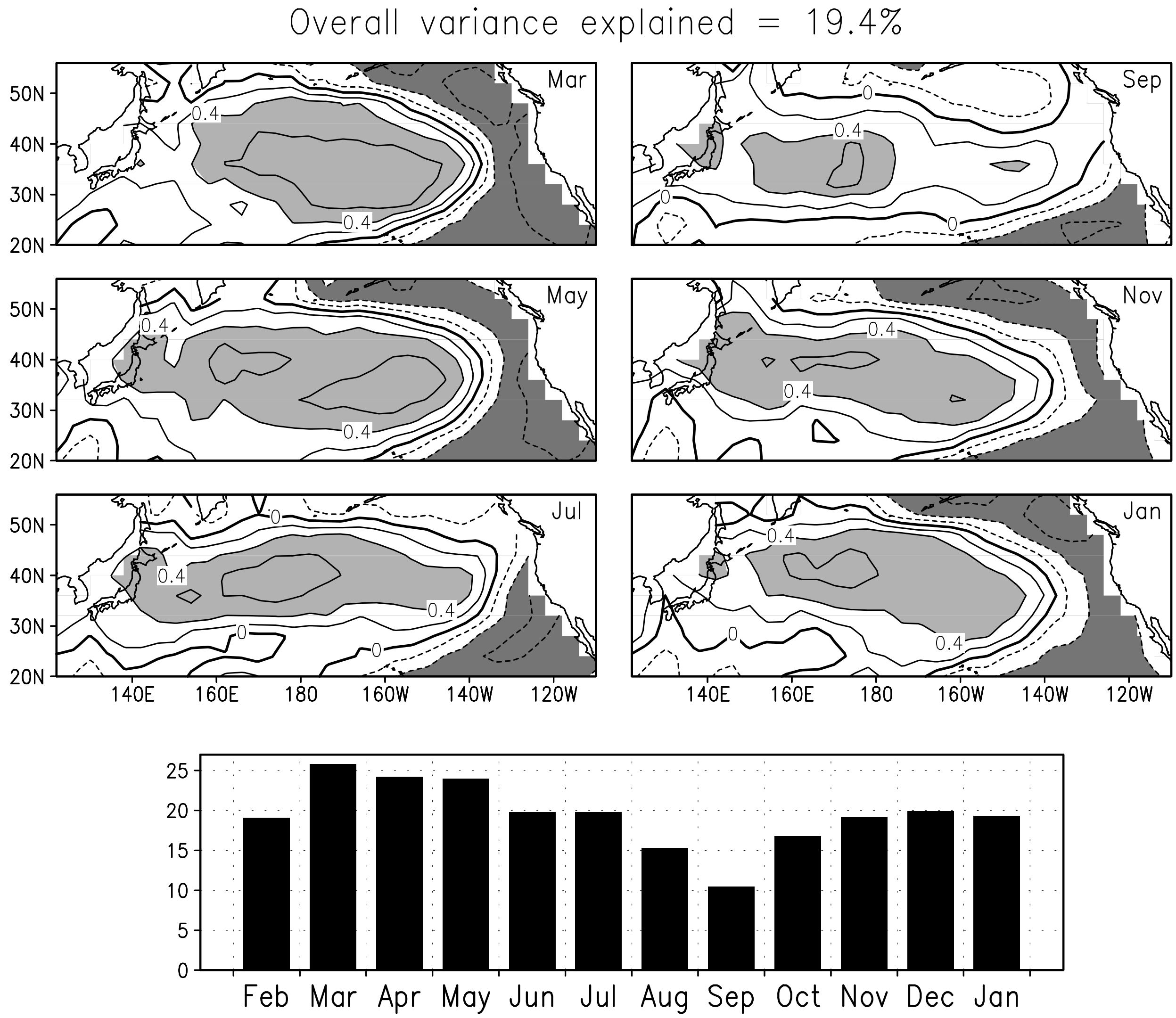

Fig. 2. Correlations between the timeseries of EEOF 1 of monthly SST anomalies from February through the following January, lags of 0-11 months, with the SST anomalies at individual gridpoints. The results are calculated using a normalized (see text) covariance matrix and presented for every other month beginning in March in a). EEOF 1 explains 19.4% of the total variance; the percent variance explained by this EEOF in each month is shown in b). The EEOF is derived from the Smith dataset for the years (1950-1996). The contour interval is 0.2, the zero contour is thick, negative contours are dashed, and values greater (less) than 0.4 (-0.4) are shaded light (dark).

functions. EEOFS, an extension of conventional EOF analysis but with time lags included in the covariance matrix, have been used by Weare and Nasstrom (1982), Lau and Chan (1985) and Lau et al. (1992) to study how patterns evolve with time. Here, EEOF analysis has been conducted using the monthly SST anomalies between February and the following January, lags of 0-11 months, from the Smith dataset. The leading EEOF is computed using the covariance matrix in which the variance at each point in a month has been normalized by the average standard deviation of SST at all points in the domain during that month. Given that the basin average standard deviation varies only slightly from a minimum 0.54 in February to a maximum of 0.70 in July, the normalized and non-normalized EEOF 1 (not shown) are very similar. The patterns associated with EEOF 1 are displayed in Fig. 2a as the correlations between the time series of EEOF 1 and time series of SST anomalies at individual grid points for the years 1950-1996. The results are presented for every other month beginning in March and indicate the temporal evolution of SST anomalies over the course of the seasonal cycle; the alternate months (not shown) indicate a similar evolution of the SST anomaly field. The dominant pattern in all months is anomalies of

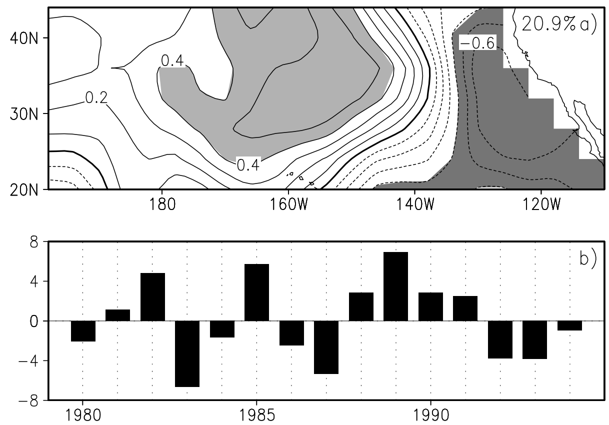

Fig. 3. a) The first EOF of the anomalous temperature field during August-September between 65-85 m depth and b) its associated principal component in the NCEP data (NPC1) for the years 1980-95. EOF 1, based on the covariance matrix, is displayed as the correlation between NPC1 and the original data. The EOF domain is 20˚N-44˚N and east of 160˚E in the North Pacific. The correlations have been smoothed with a 1-2-1 filter in both the zonal and meridional directions. The contour interval is 0.1, shading and contour options are the same as in Fig. 2.

one sign that extend from Japan to about 140°W between approximately 30°N-50°N ringed by anomalies of the opposite sign. However, the location and magnitude of the anomaly centers change with time. In winter and late spring the largest positive correlations are found in the central Pacific while the magnitude of negative correlations are greatest along the coast of North America. Through the summer the magnitude of the correlations decrease in both locations, and by September they only exceed |0.4| (shaded areas) west of 170°W between 32°-42°N, in a very small region near 38°N, 145°W, and in the very southeast corner of the domain. By November and through January higher correlation values are found over most of the area where they occurred in the previous May.

The percent variance of the SST anomalies over the North Pacific explained by this EEOF in each calendar month[1] is shown in Fig. 2b. EEOF 1 explains roughly 25% of the variance from March through May. The variance explained decreases over the next several months to a minimum of ~11% in September and then increases to about 22% from December-January.

Fig. 2 indicates that the SST anomalies in March-May are more strongly related to those in the following November-January than to the SST anomalies in the intervening summer months, especially in the eastern part of the basin. We have repeated the EEOF analyses using SST anomalies east of 160°E (not shown). The leading EEOF in this domain explains more of the total variance (21.6%), while the percent variance explained is enhanced in March-May (~32%) and November-January (~22%) and slightly diminished in September (10%), compared with the basin-wide analyses.

We next use the temperature fields from the NCEP ocean data analyses system for the period 1980-95, to examine the relationship between temperature anomalies (T') at the surface and in the summer seasonal thermocline east of 160°E in the North Pacific. The leading EOF of T' during August-September between 65-85 m depth, is used to identify the dominant pattern of variability in the center of the summer seasonal thermocline. The EOF is presented in Fig. 3a as the correlation between the leading principal component in the NCEP data (NPC1), the time series associated with EOF 1, and the values of T' at the individual grid points. EOF 1 explains 21% of the variance and has a dipole pattern with anomalies of one sign in the east-central Pacific and the opposite sign along the coast of North America. The magnitude of the correlation coefficients exceed 0.4 in much of the central and east Pacific with maxima of more than 0.6 in the dipole centers. NPC1 (Fig. 3b), shows interannual variability over the fifteen year period but no clear trend.

Correlations between NPC1 with SST anomalies at individual grid points over the North Pacific during the previous April, concurrent September, and following November are shown in Fig. 4. Regions of relatively strong correlations (>|0.4|) are shaded and used to asses the strength of the relationship between the large scale pattern of T' in the summer thermocline and SST anomalies in spring, summer, and fall. The correlations between NPC1 and SSTs in April have a dipole pattern with values that exceed 0.4 west of 140°W between 25-40°N and are less than -0.4 along the west coast of the North America. The correlation values exceed 0.8 in the vicinity of 35°N, 165°W indicating a very strong connection between the SST anomalies in spring and the T' pattern in the summer seasonal thermocline. Indeed, these correlations in the central Pacific are stronger than those between NPC1 and the T' at 65-85 m in August-September (Fig. 3a) on which this PC was originally based. The magnitude of the correlations between NPC1 and SSTs

[1] The percent variance explained is calculated using

$$\sum_{i=1}^{N} r_i^2 \sigma_i^2 / \sum_{i=1}^{N} \sigma_i^2 ,$$

where r is the correlation between SST and the timeseries of EEOF 1, σ is the standard deviation of SST, i indicates an individual grid point, and N is the total number of grid points.

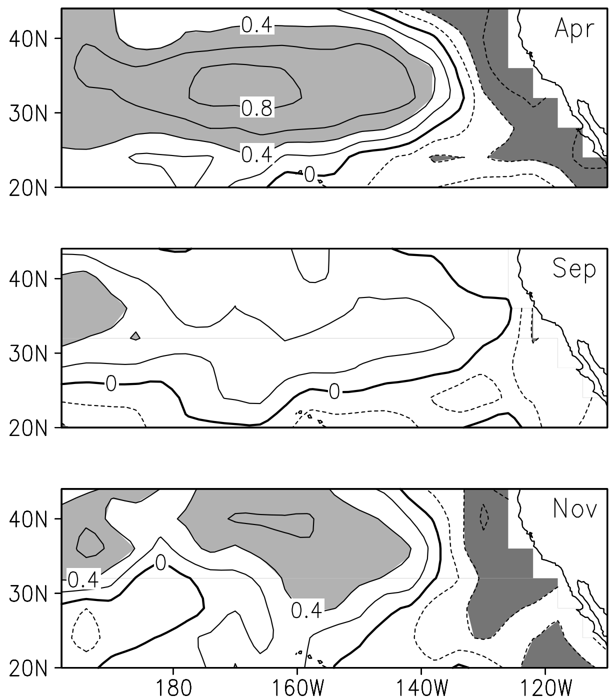

Fig. 4. Correlations between NPC1, the timeseries of dominant temperature anomaly pattern in the summer seasonal thermocline, and gridded SST anomalies from the NCEP analyses in (a) April, (b) September, and (c) November of the same year. Contours and shading are the same as in Fig. 2.

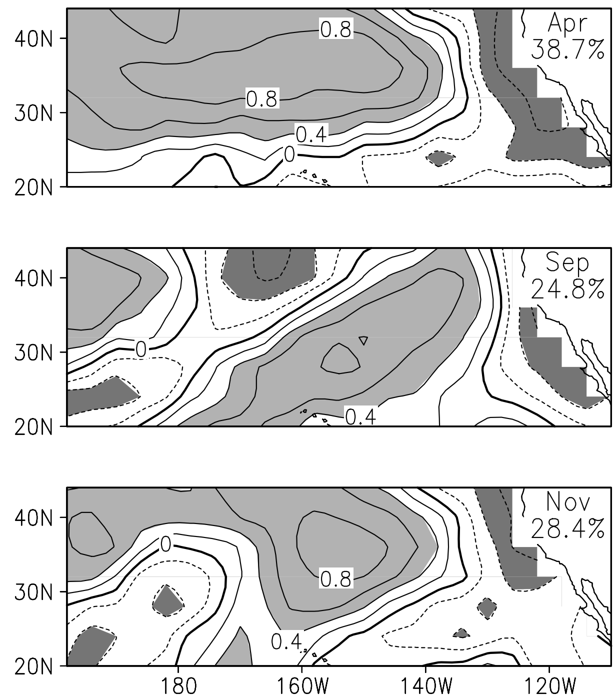

Fig. 5. EOF 1 of SST anomalies during (a) April, (b) September, and (c) November from the NCEP analyses, which explain 39%, 25% and 29% of the variance in their respective months, are shown in correlation form. Contours and shading are the same as in Fig. 2.

are small over most of the domain in September (Fig. 4b), but increase by November (Fig. 4c), exceeding 0.4 over portions of the west, central, and eastern part of the domain. These results suggest that the SST anomalies in spring descend into the seasonal thermocline and re-emerge at the surface in the following fall without persisting through summer; however, the re-emerging signal is weaker and has a slightly different pattern than the one which descends in spring. Several other processes may influence the seasonal evolution of T', including diffusion into the deeper ocean, redistribution via horizontal advection and eddy mixing, and anomalous surface energy fluxes in the second half of the year which create independent SST anomalies.

The first EOF of SST' computed separately for the months of April, September, and November using the NCEP analyses (Fig. 5) explain 38.7%, 24.8% and 28.4% of the variance, respectively. Comparing the three EOF patterns in Fig. 5 with the corresponding NPC1 - SST correlation fields in Fig. 4 indicates the extent to which the SST' pattern associated with T' in the summer thermocline resembles the dominant pattern of SST variability in spring, summer, and fall: EOF 1 bears a strong resemblance to the corresponding NPC1 - SST correlation map in April and November but not September. The similarity between the EOFs and the correlation maps for the corresponding month is quantified using pattern correlations; the two fields have a pattern correlation of 0.94, 0.45, and 0.91 in April, September, and November. The map of correlations between NPC1 and SSTs in September (Fig. 4b) does not bear a strong resemblance to any of the five leading EOFs in September: the greatest pattern correlation, 0.54, is obtained with the fourth EOF.

The percent variance of the SST anomalies explained by NPC1 between 20°N-44°N and east of 160°E in the North Pacific as a function of calendar month is shown in

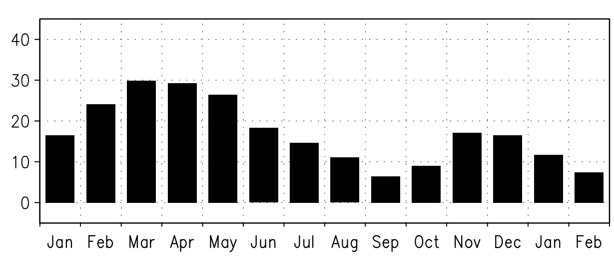

Fig. 6. The percent variance of the NCEP SST anomalies between 20˚N-44˚N and east of 160˚E in the Pacific explained by NPC1, as a function of calendar month, from the previous January to the following February for the period 1980-94.

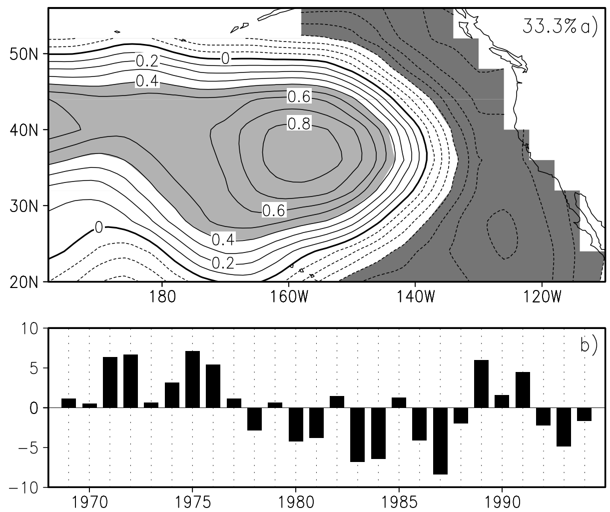

Fig. 7. (a) The first EOF of the anomalous temperature field during August-September between 60-80 m depth and (b) its associated principal component from the White data (WPC1) for the years 1969-94. The EOF domain is 20˚N-56˚N and east of 160˚E in the North Pacific. The correlations are smoothed with a 1-2-1 filter in both the zonal and meridional directions. Contours and shading are the same as in Fig. 3.

Fig. 6. The percent of the SST variance explained by NPC1 increases from about 17% in January to 30% in March and then decreases in each of the subsequent months, reaching a minimum of 6% in September (Fig. 6). It rebounds to 17% by November and then decreases through the following February. A similar representation of the timing of the re-emergence mechanism is obtained from correlations between NPC1 and the first PC of SST for each calendar month (Timlin et al. 1997), although the correlation in November, ~0.75, is nearly as large as those from February through May.

We have repeated the analyses shown in Figs. 4-6 using the White (1995) dataset to estimate T' in the summer thermocline in order to expand the domain in both space and time and to confirm the results obtained using the NCEP analyses. However, White's optimum interpolation scheme tends to smooth out monthly features, since it was designed to resolve gyre-scale temperature anomalies on seasonal or longer timescales. Temperature anomalies in the summer seasonal thermocline generally persist for at least 3 months, while the temperature anomalies at the surface can change fairly rapidly, especially in fall. Thus, we compare T' in the seasonal thermocline from the White data, with monthly SST anomalies from the Smith dataset to better resolve the re-emergence mechanism.

The leading EOF and PC of temperature anomalies averaged over 60-80 m during August-September north of 20°N and east of 160°E in the Pacific are computed from the White data for the period 1969-1994 and shown in Fig. 7. The EOF domain extends 12° farther north and the time record begins 11 years earlier than the NCEP analyses. The first EOF, which explains 33% of the variance, has one sign in the central Pacific, ringed by values of the opposite sign. The magnitude of the EOF correlation values exceed 0.4 west of 145°W near 40°N and along the North American coast, and 0.8 in the vicinity of 35°N, 160°E and just west of British Columbia. In addition to interannual variability, the first principal component at depth in summer from White (WPC1), exhibits a low frequency component with all positive values from 1969-1977 and primarily negative values from 1978-88. This "transition" in the climate state of the North Pacific in 1977 has been documented in many other studies (e.g. Trenberth and Horel 1994; Deser et al. 1996; Cayan et al. 1996).

The correlations between WPC1 with the North Pacific SST anomalies from Smith's dataset during April, September, and November are shown in Fig. 8. The three

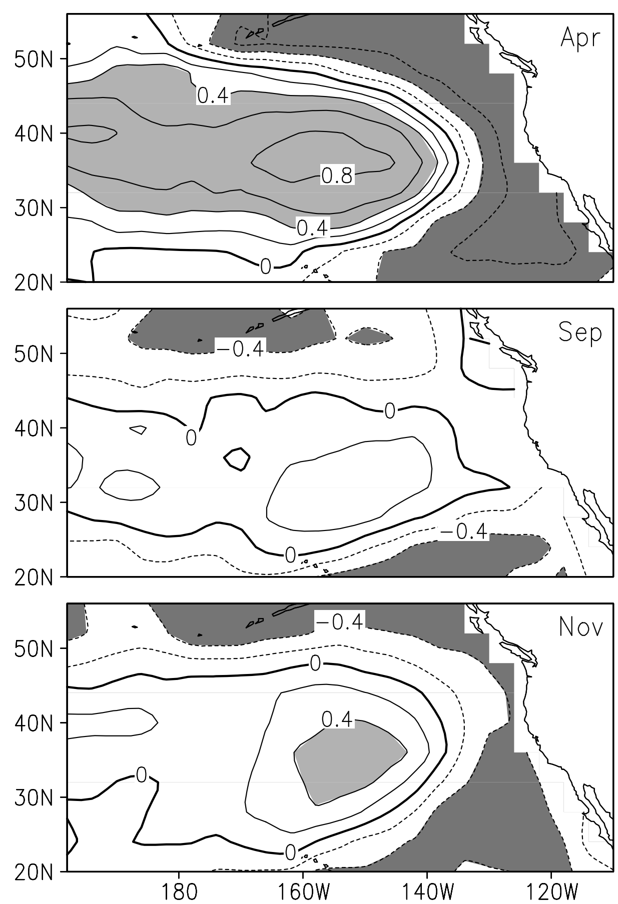

Fig. 8. Correlations between WPC1, and gridded SST anomalies from the Smith analyses in (a) April, (b) September, and (c) November for the years 1969-94. Contours and shading are the same as in Fig. 2.

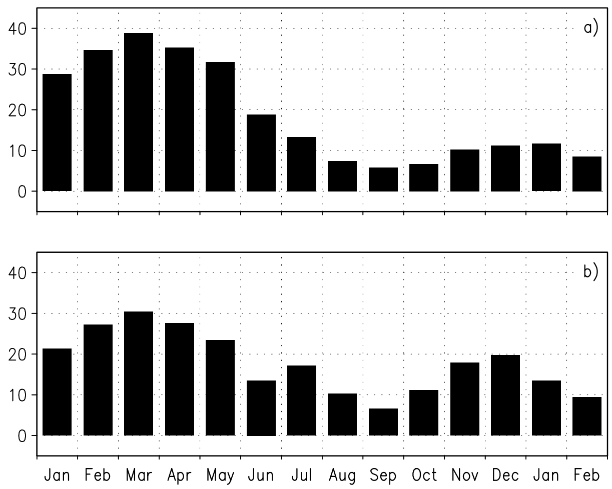

Fig. 9. The percent variance of the Reynolds SST anomalies between 20˚N-56˚N and east of 160˚E in the Pacific explained by WPC1, as a function of calendar month, from the previous January to the following February for the period (a) 1969-94 and (b) 1980-94.

correlation maps resemble their counterparts from the NCEP analyses (Fig. 4) both in pattern and in the relative strengths of the correlations where the two overlap. The absolute values of the correlations in the main centers of action are very strong in April, weak in September and moderately strong in November. The correlation maps in Fig. 8 resemble the leading EOFs of monthly SST' obtained from Smith (not shown but calculated for the same period as the White data, 1969-94) in April and November but not September. The pattern correlations between the correlation maps and the corresponding EOFs are 0.99 in April, 0.59 in September, and 0.79 in November.

The percent variance of monthly SST anomalies explained by WPC1 from January through February of the following year for the period 1969-94 (Fig. 9a) emphasize the asymmetric nature of the re-emergence mechanism: it reaches a maximum of ~40% in March, decreases to 5% by September, but only rebounds to about 10-12% from November-January. While there are several possible reasons why the connection between T' in the summer thermocline and the SST anomalies is stronger in spring than in fall, one appears to be the period of record. When we repeated the percent variance calculation using the Smith SST and WPC1 values from 1980-94, the same period as available from NCEP analysis, the explained SST variance decreases by ~1/4 of its original value in February-May and nearly doubles in November-December, becoming more symmetric about the summertime minimum (Fig. 9b), which is very similar to the results based on the NCEP data (Fig. 6). The fairly large values in late fall/early winter are maintained if we extend the period of record back to 1977 but not before (not shown), suggesting that the basin-wide climate transition in the winter of 1976-77 disrupted the re-emergence of temperature anomalies.

b. local and regional analyses

The basin-wide analyses suggest that the re-emergence mechanism is strong across much of the North Pacific at 40°N (see Figs. 1, 4, and 8). The local evolution of the re-emergence process is examined by correlating temperature anomalies at 65-85 m depth in September-August with SST anomalies over the seasonal cycle in each 4°x4° grid box in the NCEP analyses along 40°N (Fig. 10). The correlations are presented as a function of lead/lag from the previous January (SSTs lead by ~7.5 months) to the following April (SST lags by ~7.5 months). Evidence for the re-emergence mechanism is clearly seen east of ~160°E. High correlations (> 0.6) from the previous Feb-May decrease to a minimum in August-September (< 0.4) and then increase in the following fall and/or winter (>

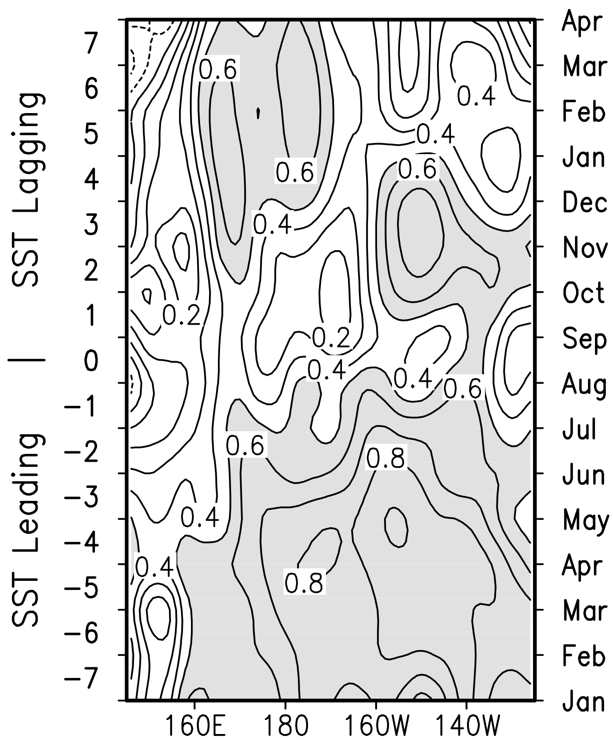

Fig. 10: Lead-lag correlations between temperature anomalies located between 65-85 m in August-September, and SST anomalies from the previous January through the following April for each grid box along 40°N. For example, the correlation between SST in the previous May (SST leads by 3.5 months) and temperature anomalies in the summer thermocline is ~0.9 at 160˚W. The temperature anomalies are from the NCEP analyses for the period 1980-95. The correlation values have been smoothed longitudinally using a 1-2-1 filter, the contour interval is 0.1, and values greater than 0.5 are shaded.

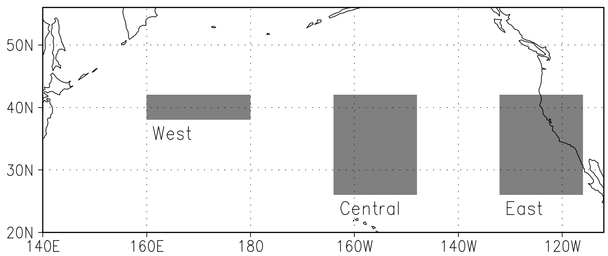

Fig. 11. Shaded areas indicate the eastern (26N°-42°N, 132°W-116°W), central (26N°-42°N, 164°W-148°W), and western (38N°-42°N, 160°E-180°) regions which will be used to examine the re-emergence mechanism.

0.5). The temperature anomalies appear to return to the surface 1-3 months later between 160°E-160°W compared with the eastern Pacific. Similar analyses at other latitudes indicate that the re-emergence process is most active east of approximately 165°E and north of 28°N (not shown).

We next focus on the vertical structure of the re-emergence mechanism in regions where the basin-wide analyses suggest that the re-emergence mechanism is strong: along the North American coast in the east Pacific, north of Hawaii in the central Pacific and along 40°N in the west Pacific, as indicated by the three shaded areas in Fig. 11. Formal criteria were not used to select the exact regional boundaries; rather rectangular areas were selected to obtain a clear depiction of the re-emergence process. Following Alexander and Deser (1995), we compute the correlation between a basepoint located in summer thermocline with temperature anomalies from the previous January to the following winter from the surface down to 150 m. Temperature anomalies from the NCEP analyses between 65-85 m in August-September, the same months and depths used to calculate NPC1, are averaged together to create a basepoint timeseries. The temperature anomalies have been regionally averaged on each level and then smoothed with a 1-2-1 filter in time before performing the correlation analyses. Note that in the following figures we have chosen to shade values exceeding different contour levels in order to best illustrate the re-emerging signal.

All three regions show evidence of the re-emergence mechanism as the correlations between the basepoint and surface temperatures are high in the previous winter, drop in summer, and rebound in the following fall/winter (Fig. 12). However, the structure and timing of the correlation pattern is different in the three locations. For example, in the east Pacific the correlation between the SST and basepoint goes from a maximum of more than 0.9 in March decreases to less then 0.3 in August and exceeds 0.45 from November through February. In contrast, in the central Pacific the correlations do not decrease as strongly in summer but rapidly decline after reaching more then 0.7 in November, while in the western region high correlation values persist at the surface through much of the following winter. The correlation values in the east and central region descend from March through the following January suggesting that some of the thermal anomalies move downward into the permanent pycn-

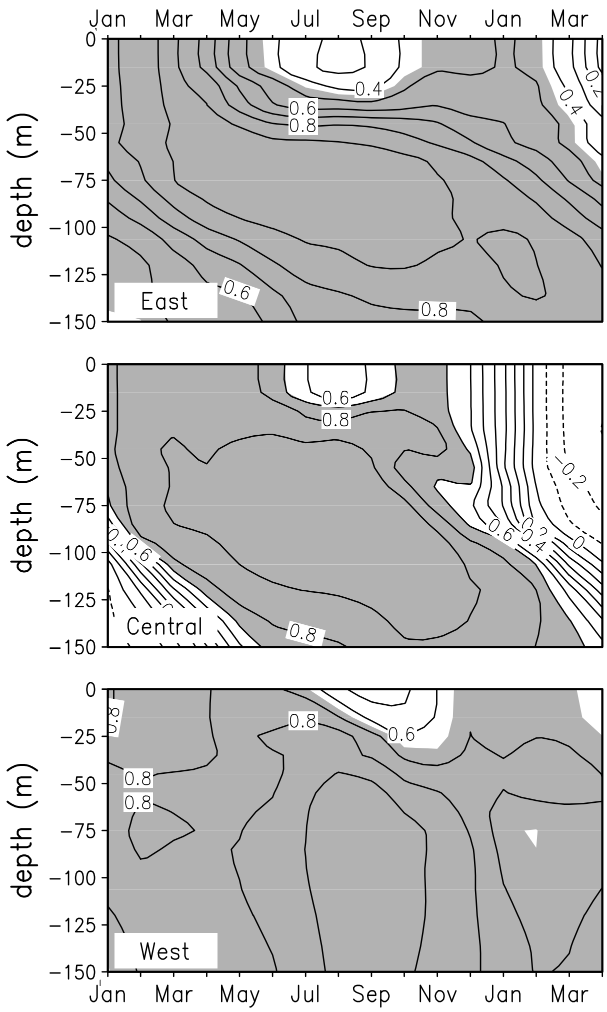

Fig. 12. Lead-lag correlations between temperature anomalies at the base point, located between 65-85 m in August-September, and temperature anomalies between the surface and 150 m from the previous January through the following April in the (a) east, (b) central and (c) west Pacific regions. The anomalies obtained from the NCEP analyses for the period 1980-95 are averaged over the region at each level and then smoothed in time using a 1-2-1 filter, the anomalies in the western region are also smoothed over depth since the signal is somewhat noisier in this small region. The contour interval is 0.1. Shading is used to highlight the re-emergence mechanism and so it varies between regions: correlations in excess of (a) 0.45, (b) 0.7, and (c) 0.65 are shaded.

ocline.

The regional behavior of the thermal anomalies is explored further by regressing the temperature anomalies as a function of month and depth on anomalies at the basepoint, located here at 5 m (the top level of the NCEP analyses and taken to represent the SST) in April-May. The regression analyses provides a linear estimate of how an SST anomaly of 1°C in spring evolves from the previous January through the following April, allowing one to track the magnitude of an anomaly through the full re-emergence process. A 1°C anomaly is fairly large, as the standard deviation of SST' in April-May is approximately 0.5, 0.6, and 0.75°C, in the east, central, and west Pacific. The regressions indicate the re-emergence mechanism occurs in all three regions but with clear differences between the three. In the eastern region, the SST anomalies in late spring appear to move downward over a fairly narrow zone (30-80 m) maintaining their magnitude through September while decreasing by more then half in the surface mixed layer over the same time. While some of the thermal anomalies continue moving down through the following winter a portion of the signal, indicated by regression values of more than 0.55°C, returns to the surface in November and December. Compared with the east Pacific, the re-emergence signal occurs earlier in the year and extends deeper in the central and especially the west Pacific. In the western region large regression values (> 0.75) extend over the upper 150 m in the first winter, persist through a deep layer in summer and then return to the surface 2-3 months later than in the other two regions.

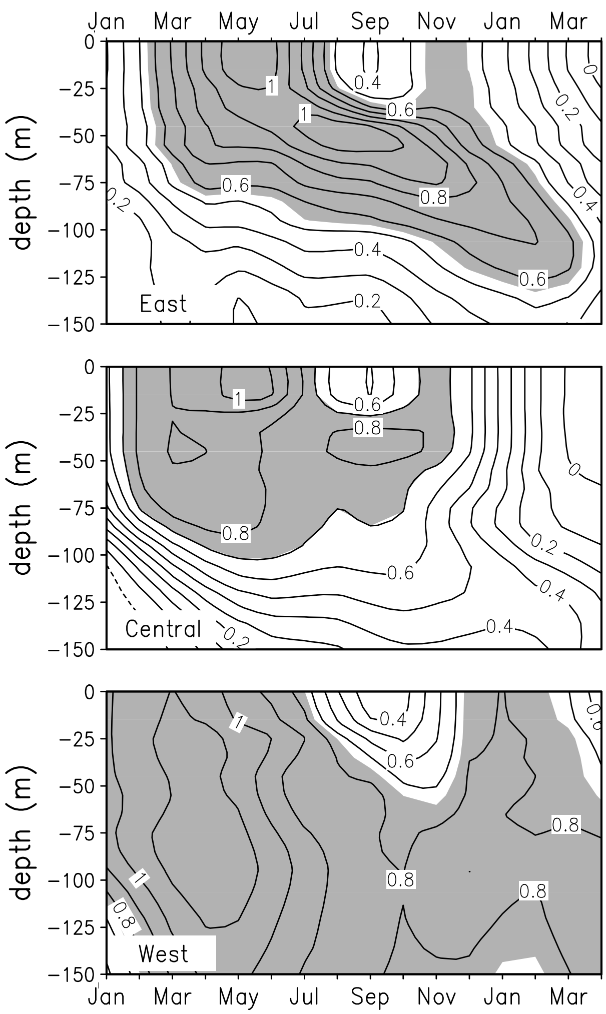

Fig. 13. As in Fig. 12 but for lead-lag regressions (˚C per 1˚C) between temperature anomalies at the base point, located here at 5 m in April-May, and temperature anomalies from the previous January through the following April in the (a) east, (b) central and (c) west Pacific regions. The contour interval is 0.1 and values greater than (a) 0.55, (b) 0.7, and (c) 0.75 are shaded.

The differences in the timing and strength of the re-emergence mechanism indicated by both the correlation and regression analyses are partly due regional variations in the mean seasonal cycle of mixed layer depth. The maximum mixed layer depth in the North Pacific, which tends to occur in March, increases from about 80 m along the west coast of North America, to 120 m in the central Pacific, and 200 m east of Japan (Bathen 1972, Yan and Okubo 1992, Deser et al. 1996). As a result the depth to which temperature anomalies penetrate in late winter increases from east to west as suggested by Fig. 13. The mixed layer shoals to ~25 m in during summer in all three regions and thus the vertical extent of T' below the mixed layer is greater in the west than the east. When the mixed layer deepens in the following fall the anomalies are generally closer to the surface and thus incorporated into the mixed layer sooner in the east and central compared with the west Pacific.

The timing of the re-emergence mechanism differs slightly in the correlation and regression analyses. For example, in the eastern region the correlation analyses suggest that the strongest return of T' to the surface occurs in January while the regression analyses indicate that the return is strongest in November; the latter is consistent with most of the basin-wide analyses. One reason for differences between the two analysis methods is that correlations depend on the variance of both the basepoint and the other timeseries while the regressions depend only on the former. Thus, the seasonal cycle of the background variability in the upper ocean and the position of the basepoint relative to this variability will influence how the two methods portray the re-emergence mechanism. A second factor relates to the position of the basepoint relative to the path of the re-emergence mechanism. The correlation analyses maximize the portion of the signal which passes through 65-85 m in August-September, while the regression analyses indicate that in the eastern region the strongest thermal anomalies that descend from the surface in April-May are located at ~50 m during the summer.

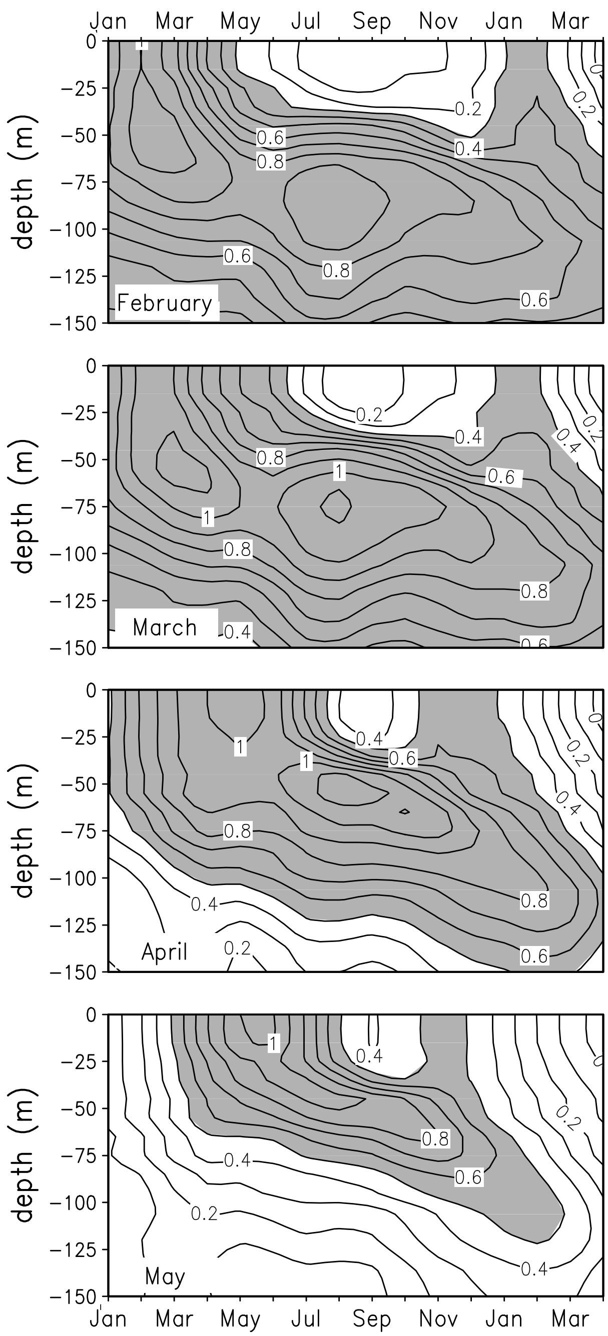

Fig. 14. As in Fig. 13 but for lead-lag regressions (˚C per 1˚C) in the eastern region between temperature anomalies at the base point, located at 5 m in (a) February (b) March, (c) April and (d) May. The contour interval is 0.1 and values greater than (a) 0.3, (b) 0.4, (c) 0.5 and (d) 0.5 are shaded.

We explore the possibility of different paths for the re-emerging anomalies by computing lead-lag temperature regressions in the eastern region, similar to Fig. 13a, but with a surface basepoint which progress from February through May. Advancing the basepoint from February to May progressively shortens and shallows the path of the re-emergence mechanism (Fig. 14). With a February basepoint, the center of the re-emergence signal penetrates to ~80 m by the following month and then is maintained between 70-100 m through summer and into early fall before returning to the surface in January-February of the following year. With a May basepoint the initial SST signal moves slowly downward, at a rate of 5-10 m per month, and is concentrated near 50 m in summer before returning to the surface in November. The SST anomalies in summer also experience a greater decrease when the re-emergence process begins earlier in the year, but the signal which re-emerges in the following fall/winter is ~0.2°C relative to the summer minimum in all four cases. Comparing the evolution of SST' in the top and bottom panels in Fig. 14 indicate that a 1°C anomaly in February (May) decays to 0.1°C (0.4°C) by September but then increases to more than 0.3°C in January (0.5°C in November). Moving the surface basepoint from February through May also causes the re-emergence signal to return to the surface earlier in the year in the western Pacific but does not visibly alter the re-emerging mechanism in the central region (not shown).

4. Summary and discussion

Three gridded data sets, the SST analysis of Smith et al. (1996) and subsurface temperature analyses from NCEP’s ocean data assimilation system (Derber and Rosati 1989; Ji et al. 1995) and White’s optimum interpolation scheme (1995) are used to examine the winter-to-winter re-emergence of SST anomalies in the North Pacific. We evaluate the re-emergence mechanism on a broad scale by correlating the first principal component (PC1), the time series of the leading pattern of ocean temperature anomalies in the summer seasonal thermocline (~60-85 m in August-September), with SST anomalies over the course of the year. The correlations are of one sign in the central Pacific and the opposite sign along the coast of North America, with relatively large magnitudes (> |0.4|) in April and November but are much weaker in September. Furthermore, the pattern of the correlations closely resembles the leading EOF in the April and November but not September, suggesting that the dominant large-scale SST anomaly pattern that forms in the North Pacific during late winter descend into the seasonal thermocline in summer and returns to the surface in the following fall, with limited persistence at the surface in the summer.

While the broad pattern of SST anomalies that participate in the re-emergence mechanism are driven by the large-scale atmospheric forcing, the re-emergence process itself is primarily local in nature, since advection and other horizontal processes are relatively slow in the ocean and do not have sufficient time to change the thermal patterns over the course of a year. Regions in the eastern, central, and western Pacific all show evidence of the re-emergence mechanism but differences between the three suggest that geographic variability in the mixed layer depth and the static stability of the layers below it influence the timing and structure of the re-emerging signal. The maximum mixed layer depth increases from less than 100 m near the North American coast to more than 200 m east of Japan and the permanent pycnocline below the mixed layer is strongest in the east Pacific and decreases westward. As a result, thermal anomalies are confined to a fairly narrow summer seasonal thermocline in the east compared with the west. For SST anomalies initiated at the same time, those in the east and central Pacific tend to be re-entrained into the mixed layer by November-December compared to the west, where mixed layer deepening continues to entrain the thermal anomalies into January-February of the following year.

The re-emerging mechanism at a given location is also influenced by when the SST anomalies are created and how long they persist at the surface. SST anomalies that are initiated in February-March extend through a relatively deep mixed layer, persist at greater depths in summer, and are then re-entrained later in the year compared with those initiated in April-May. The anomalies created in late spring tend to pass through the upper part of the seasonal thermocline in summer before returning to the surface around November. Thus, the path of the re-emerging signal maybe more variable where SST anomalies change from winter to spring compared to regions where SST anomalies in the first half of the year are more persistent. The greater persistence of SST anomalies in the first half of the year in the central Pacific might help explain why the evolution of the re-emergence mechanism was less sensitive to when the SST anomaly was initiated there compared with regions located in the east or west Pacific.

Most of the statistical analyses used here indicate that the descending branch of the re-emergence mechanism is stronger than the return branch, i.e. the SST anomalies in the previous winter/spring are more strongly connected to the temperature anomalies in the summer thermocline than the SST anomalies in the following fall/winter. For example, PC1 in the summer seasonal thermocline explains 30%/6%/17% of the SST variability over the North Pacific in April/September/November in the NCEP dataset for the years 1980-1995. The asymmetry in the percent variance explained is even greater using PC1 from White's data and the SSTs from Smith for the years 1969-94. Regional analyses suggest that for an initial SST anomaly of 1°C the temperature anomalies that return to the surface in fall/winter range between 0.3-0.8°C, which is 0.2-0.4°C greater than the summer minimum (Figs. 12 and 13). However, comparing the fall and summer SST anomalies directly underestimates the impact of the re-emergence mechanism, since SST anomalies decay due to negative air-sea feedbacks. In the absence of other processes, SST anomalies decay at a rate of $\exp(-\tau/\lambda)$ where τ is the lag in months and λ, the constant air-sea damping factor, is on the order of 3-6 months (Frankignoul and Hasselmann 1977; Alexander and Penland 1996; and Lau and Nath 1996). Depending on the value of λ and the length of time between the summer minimum (September) and the fall/winter maximum (November-February), the re-emergence mechanism provides an additional 0.1-0.3°C of heating to the surface layer to compensate for the heat loss associated with surface fluxes.

The relative strength of the descending and return branches of the re-emergence mechanism are likely due to differences in the mixed layer physics over the course of the year. In the descending branch the anomalies created at the surface are left behind when the mixed layer retreats and then incorporated into the stable seasonal thermocline, a relatively passive process. Over the next few months some of the thermal anomalies are diffused to deeper layers, or mixed by eddies before being entrained into the mixed layer. In addition, other processes active in the surface layer such as air-sea heat fluxes and Ekman transport may influence SST anomalies, diluting the re-emerging signal in the following fall and winter.

The re-emergence mechanism is just one of several processes which influence SST variability on interannual and longer timescales. Winter-to-winter persistence of SST anomalies may also result from persistence of wintertime atmospheric circulation patterns via surface heat fluxes. Indeed, there is some evidence from observations (Namias 1986, Namias et al. 1988) and atmospheric GCM experiments with fixed SST boundary conditions (Ting and Lau 1983, Graham et al. 1994, Lau 1997) that circulation anomalies recur from one winter to the next. To examine this possibility, we correlated the surface heat fluxes in winter/spring with those in the following fall/winter at each grid point over the North Pacific. The results (not shown) indicate that the correlations between

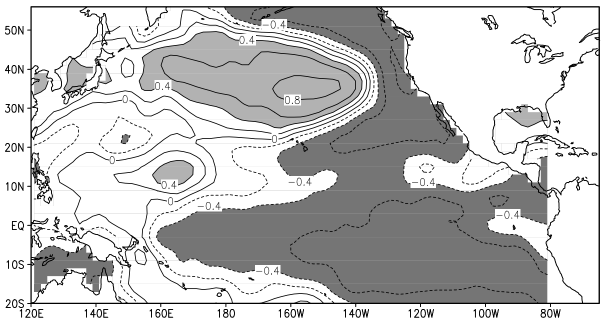

Fig. 15. Correlations between PC1 obtained from White's analyses, and SST anomalies during March at individual gridpoints from Smith et al. for the years 1969-94. The correlations have been smoothed with a 1-2-1 filter in both the zonal and meridional directions. Contours and shading are the same as in Fig. 2.

the anomalous fluxes in March-April-May and the following October-November-December are negative over much of the eastern half of the basin and less than 0.3 over almost all of the North Pacific in the NCEP reanalysis (described by Kalnay et al. 1996) for the years 1969-94. In places where there is winter-to-winter forcing of SST anomalies by the atmosphere, the re-emergence mechanism would likely act to amplify and lengthen the period of the SST anomalies.

In an apparent contradiction to our findings and those of Namias et al. 1988, Zhang et al. (1998) have suggested that SST anomalies in the North Pacific persist from winter to summer and summer to winter. Norris et al. (1998) attribute this persistence to positive feedbacks between low-level stratiform clouds and SSTs. It is possible that both persistence at the surface and the re-emergence mechanism may be operating in the North Pacific but the different data and analyses methods emphasize different aspects of the SST variability. For example, while the autocorrelation of the timeseries of the leading pattern of SST in Zhang et al. (their Fig. 7a) does suggest persistence of summertime SST anomalies, it also provides evidence for the re-emergence mechanism, as indicated by an increase in autocorrelation after lags of 8-10 months for SST anomalies that existed in January through April. Extended EOF analyses of SST anomalies during each calendar month (our Fig. 2) also suggests that both processes operate in the North Pacific: the anomaly center located along 40°N in the central and west Pacific shows some tendency to persist throughout the year, while in other regions, especially east of the dateline, SST anomalies in spring diminish in summer and then increase again in fall and early winter.

Many studies have shown a connection between the El Niño/Southern Oscillation (ENSO) phenomena and SST anomalies in the eastern half of the North Pacific (e.g. Weare et al. 1976; Pan and Oort 1990; Deser and Blackmon 1995). Fig. 15 shows the correlation pattern of March SSTs with the leading PC of subsurface temperature anomalies in summer obtained from the White data for the years 1969-94. The correlation pattern is consistent with SST anomalies during ENSO: temperature anomalies in the summer thermocline in the central North Pacific are strongly correlated with local SSTs and anticorrelated with SSTs along the coast of North America and the eastern tropical Pacific in the previous March. The high correlations (>0.6) in the eastern tropical Pacific suggest a fairly strong connection between ENSO and the North Pacific temperature anomaly pattern involved in the re-emergence mechanism.

The SST anomalies in the tropical Pacific in winter and spring and the subsurface temperature anomalies in the North Pacific in summer are linked via two processes. First, during El Niño events enhanced convection over the warm SST anomalies in central equatorial Pacific leads to a change in the atmospheric circulation including an enhancement of the Aleutian low in winter which in turn forces SST anomalies to form in the North Pacific (Alexander 1990, 1992; Luksch et al. 1990; Lau and Nath 1996). The SST anomaly pattern in the North Pacific, which takes one to two months to develop, then enters the seasonal thermocline in late winter and early spring via the second process, the descending branch of the re-emergence mechanism. The extent to which the atmosphere responds to the ocean temperature anomalies which return to the surface in the North Pacific in the following fall and winter remains an open question.

Acknowledgments

We thank Thomas Smith, Richard Reynolds, Ants Leetmaa, and Ming Ji at NCEP and Warren White of Scripps Institute of Oceanography for providing the ocean temperature analyses. We also benefited from discussions with Art Miller. This work was supported by NSF grant OCE-9531870 and by an omnibus grant from the NOAA office of global programs to the Climate Diagnostics Center.

REFERENCES

Alexander, M. A., 1990: Simulation of the response of the North Pacific Ocean to the anomalous atmospheric circulation associated with El Niño. *Climate Dyn.*, **5**, 53-65.

Alexander, M. A., 1992: Midlatitude atmosphere-ocean interaction during El Niño. Part I: the North Pacific Ocean. *J. Climate*, **5**, 944-958.

Alexander, M. A., and C. Deser, 1995: A mechanism for the recurrence of wintertime midlatitude SST anomalies. *J.*

Phys. Oceanogr., **25**, 122-137.

Alexander, M. A. and C. Penland, 1996: Variability in a mixed layer model of the upper ocean driven by stochastic atmospheric surface fluxes. *J. Climate*, **9**, 2424-2442.

Barsugli, J. J. and D. S. Battisti, 1997: The basic effects of atmosphere-ocean thermal coupling on midlatitude variability. *J. Atmos. Sci.*, in press.

Battisti, D. S., U. S. Bhatt and M. A. Alexander, 1995: A modeling study of the interannual variability in the wintertime North Atlantic Ocean. *J. Climate*, **8**, 3067-3083.

Bhatt, U. S., M. A. Alexander, D. S. Battisti, D. D. Houghton and L. M. Keller, 1997: Role of atmosphere-ocean interaction in North Atlantic climate variability. *J. Climate*, in press.

Blade, I., 1997: The influence of midlatitude coupling on the low frequency variability of a GCM. Part I: No tropical SST forcing. *J. Climate*, **10**, 2087-2106.

Capatondi, A. and W. R. Holland, 1997: Decadal variability in an idealized ocean model and its sensitivity to surface boundary conditions. *J. Phys. Oceanogr.*, **27**, 1072-1093.

Cayan, D. R., A. J. Miller, T. P. Barnett, N. E. Graham, J. N. Ritchie and J. M. Oberhuber, 1996: Seasonal-interannual fluctuations in surface temperature over the Pacific: effects of monthly winds and heat fluxes. *Natural Climate Variability on decade-to-century timescales.*, National Academy of Sciences Press, 133-150.

Delworth, T., 1996: North Atlantic interannual variability in a coupled ocean-atmosphere model. *J. Climate*, **9**, 2356-2375.

Delworth, T., S. Manabe and R. J. Stouffer, 1993: Interdecadal variations of the thermohaline circulation in a coupled ocean-atmosphere model. *J. Climate*, **6**, 1993-2011.

Derber, J. D. and A. Rosati, 1989: A global oceanic data assimilation system. *J. Phys. Oceangr.*, **19**, 1333-1347.

Deser, C., M. A. Alexander and M. S. Timlin, 1996: Upper ocean thermal variations in the North Pacific during 1970 - 1991. *J. Climate*, **9**, 1841-1855.

Deser, C. and M. L. Blackmon, 1995: On the relationship between tropical and north Pacific sea surface temperature variations. *J. Climate*, **8**, 1677-1680.

Elsberry, R. and R. W. Garwood, 1978: Sea surface temperature anomaly generation in relation to atmospheric storms. *Bull. Amer. Meteor. Soc.*, **59**, 786-789.

Frankignoul, C., 1985: Sea surface temperature anomalies, planetary waves, and air-sea feedback in the middle latitudes. *Rev. Geophys.*, **23**, 357-390.

Frankignoul, C. and K. Hasselmann, 1977: Stochastic climate models. Part 2. Application to sea-surface temperature variability and thermocline variability. *Tellus*, **29**, 284-305.

Frankignoul, C. and R. W. Reynolds, 1983: Testing a dynamical model for mid-latitude sea surface temperature anomalies. *J. Phys. Oceanogr.*, **13**, 1131-1145.

Frankignoul, C., P. M¸ller and E. Zorita, 1997: A simple model of the decadal response of the ocean to stochastic wind forcing. *J. Phys. Oceanogr.*, submitted.

Gill, A. E. and P. P. Niiler, 1973: The theory of the seasonal variability in the ocean. *Deep Sea Res.*, **20**, 141-177.

Graham, N. E., T. P. Barnett, R. Wilde, M. Ponater and S. Schubert, 1994: On the roles of tropical and midlatitude SSTs in forcing annual to interdecadal variability in the winter Northern Hemisphere circulation. *J. Climate*, **7**, 1416-1442.

Gu, D. and S. G. H. Philander, 1997: Interdecadal climate fluctuations that depend on exchanges between the tropics and extratropics. *Science*, **275**, 805-807.

Hall, A. and S. Manabe, 1997: Can local linear stochastic theory explain sea surface temperature and salinity variability. *Climate Dyn.*, **13**, 167-180.

Jacobs, G. A., H. E. Hurlburt, J. C. Kindle, E. J. Metzger, J. L. Mitchell and A. J. Wallcraft, 1994: Decade-scale trans-Pacific propagation and warming effects of an El Niño anomaly. *Nature*, **370**, 360-363.

Ji, M., A. Leetmaa and J. Derber, 1995: An ocean analyses system for seasonal to interannual climate studies. *Mon. Wea. Rev.*, **123**, 460-480.

Kalnay, E. and Coauthors, 1996: The NCEP/NCAR 40-year reanalysis project. *Bull. Amer. Meteor. Soc.*, **77**, 437-471.

Klein, S. A., D. L. Hartmann and J. R. Norris, 1995: On the relationships among low-cloud structure, sea surface temperature and atmospheric circulation in the summertime northeast Pacific. *J. Climate*, **8**, 1140-1155.

Lanzante, J. R. and R. P. Harnack, 1983: An investigation of summer sea surface temperature anomalies in the eastern North Pacific Ocean. *Tellus*, **35A**, 256-268.

Latif, M. and T. P. Barnett, 1994: Causes of decadal climate variability over the North Pacific and North America. *Science*, **266**, 634-637.

Latif, M. and T. P. Barnett, 1996: Decadal climate variability over the North Pacific and North America: dynamics and predictability. *J. Climate*, **9**, 2407-2423.

Lau, K. M. and P. H. Chan, 1985: Aspects of the 40-50 day oscillation during the northern winter as inferred from outgoing longwave radiation. *Mon. Wea. Rev.*, **113**, 1889-1909.

Lau, N.-C., 1997: Interactions between global sst anomalies and the midlatitude atmospheric circulation. *Bull. Amer. Meteor. Soc.*, **78**, 21-33.

Lau, N. C., S. G. H. Philander and M. J. Nath, 1992: Simulation of ENSO-like phenomena with a low-resolution coupled GCM of the global ocean and atmosphere. *J. Climate*, **5**, 284-307.

Lau, N.-C. and M. J. Nath, 1996: The role of the 'atmospheric bridge' in linking tropical Pacific ENSO events to extratropical SST anomalies. *J. Climate*, **9**, 2036-2057.

Luksch, U., H.v.Storch and E. Maier-Reimer, 1990: Modeling North Pacific SST anomalies as a response to anomalous atmospheric forcing. *J. Mar. Syst.*, **1**, 51-60.

Mantua, N. J., S. R. Hare, Y. Zhang, J. M. Wallace and R. Francis, 1997: A Pacific interdecadal climate oscillation with impacts on salmon production. *Bull. Amer. Meteor. Soc.*, **78**, 1069-1079.

Meyers, S. D., M. A. Johnson, M. Liu, J. J. O'Brien and J. L. Spiesberger, 1996: Interdecadal variability in a numerical model of the northeast Pacific Ocean:1970-89. *J. Phys. Oceanogr.*, **26**, 2635-2652.

Miller, A. J., D. R. Cayan and J. M. Oberhuber, 1994: On the re-emergence of midlatitude SST anomalies. *Proc. of the Proc. 18th Annual Climate Diagnostics Workshop*, Boulder, CO, USA, NOAA, 149-152.

Namias, J., 1986: Persistence of flow patterns over North America and adjacent oceans. *Mon. Wea. Rev.*, **114**, 1368-1383.

Namias, J. and R. M. Born, 1970: Temporal coherence in North Pacific sea-surface temperature patterns. *J. Geophys. Res.*, **75**, 5952-5955.

Namias, J. and R. M. Born, 1974: Further studies of temporal coherence in North Pacific sea surface temperatures. *J. Geophys. Res.*, **79**, 797-798.

Namias, J., X. Yuan and D. R. Cayan, 1988: Persistence of North Pacific sea surface temperature and the atmospheric flow patterns. *J. Climate*, **1**, 682-703.

Norris, J. R. and C. Leovy, 1994: Interannual variability in stratiform cloudiness and sea surface temperature. *J. Climate*, **7**, 1915-1925.

Norris, J. R., Y. Zhang and J. M. Wallace, 1998: Role of clouds in summertime atmosphere-ocean interactions over the North Pacific. *J. Climate*, submitted.

Pan, Y. H. and A. H. Oort, 1990: Correlation analyses between sea surface temperature anomalies in the eastern equatorial Pacific and the world ocean. *Climate Dyn.*, **4**, 191-205.

Quenouille, 1954: *Associated Measurements.* Butterworths,242 pp.

Robertson, A. W., 1996: Interdecadal variability over the North Pacific in a multi-century climate simulation. *Climate Dyn.*, **12**, 227-241.

Saravanan, R. and J. C. McWilliams, 1997: Stochasicity and spatial resonance in interdecadal climate fluctuations. *J. Climate*, **10**, 2299-2320.

Smith, T. M., R. W. Reynolds, R. E. Livezey and D. C. Stokes, 1996: Reconstruction of historical sea surface temperatures using empirical orthogonal functions. *J. Climate*, **9**, 1403-1420.

Tanimoto, Y., N. Iwasaka, K. Hanawa and Y. Toba, 1993: Characteristic variations of sea surface temperature with multiple time scales in the North Pacific. *J. Climate*, **6**, 1153-1160.

Timlin, M. S., M. A. Alexander and C. Deser, 1997: The re-emergence of midlatitude SST anomalies. *Proc. of the Proc. 21st Annual Climate Diagnostics and Prediction Workshop*, Huntsville, Alabama, NOAA, 154-156.

Ting, M. and N.-C. Lau, 1993: A diagnostic and modeling study of the monthly mean wintertime anomalies appearing in a 100-year GCM experiment. *J. Atmos. Sci.*, **50**, 2845-2867.

Trenberth, K. E. and J. W. Hurrell, 1994: Decadal atmosphere-ocean variations in the Pacific. *Climate Dyn.*, **9**, 303-319.

Weare, B., 1994: Interrelationships between cloud properties and SSTs on seasonal and interannual timescales. *J. Climate*, **7**, 248-260.

Weare, B. C. and J. S. Nasstrom, 1982: Examples of extended empirical orthogonal function analyses. *Mon. Wea. Rev.*, **110**, 481-485.

Weare, B. C., A. R. Navato and R. E. Newell, 1976: Empirical orthogonal analysis of Pacific Ocean sea surface temperatures. *J. Phys. Oceanogr.*, **6**, 671-678.

Weaver, A. J., E. S. Sarachik and J. Marotzke, 1991: Internal low frequency variability of the ocean's thermohaline circulation. *Nature*, **353**, 836-838.

White, W. B., 1995: Design of a global observing system for gyre-scale upper ocean temperature variability. *Prog. Oceanogr.*, **36**, 169-217.

Yukimoto, S., M. Endoh, Y. Kitamura, A. Kitoh, T. Motoi, A. Noda and T. Tokioka, 1996: Interannual and interdecadal variabilities in the Pacific in an MRI coupled GCM. *Climate Dyn.*, **12**, 667-683.

Zhang, R.-H. and S. Levitus, 1997: Structure and cycle of decadal variability of upper-ocean temperature in the North Pacific. *J. Climate*, **10**, 710-727.

Zhang, Y., J. M. Wallace and D. S. Battisti, 1997: ENSO-like interdecadal variability. *J. Climate*, **10**, 1004-1020.

Zhang, Y., J. R. Norris and J. M. Wallace, 1998: Seasonality of large scale atmosphere-ocean interaction over the North Pacific. *J. Climate*, submitted.

Zorita, E. and C. Frankignoul, 1997: Modes of North Atlantic decadal variability in the ECHAM1/LSG ocean-atmosphere general circulation model. *J. Climate*, **10**, 183-200.